Design and Characterization of AlGaInAs/InP Buried Heterostructure Transistor Lasers Emitting at 1.3-μm Wavelength

Noriaki Sato, Mizuki Shirao, *Member, IEEE*, Takashi Sato, Masashi Yukinari, Nobuhiko Nishiyama, *Senior Member, IEEE*, Tomohiro Amemiya, *Member, IEEE*, and Shigehisa Arai, *Fellow, IEEE*

***Abstract*—We discuss the wafer design and fabrication process for the 1.3-μm-wavelength AlGaInAs/InP transistor lasers, and the structural dependence of lasing and the electrical characteristics are shown. We particularly focus on the base structure, and the thickness and width dependence are numerically and experimentally analyzed. A thicker base layer resulted in lower optical confinement factor in the quantum wells (QWs), higher optical loss, and lower current gain. In addition, a wider base width caused leak current recombination outside the QWs. By modifying the structure of an n-p-n TL, it was possible to simultaneously realize room-temperature continuous-wave lasing and transistor operation.**

***Index Terms*—AlGaInAs/InP, quantum-well (QW) laser, transistor laser (TL).**

I. Introduction

Today, data traffic is rapidly increasing, and the demand for high-speed data transmission is strong. Optical communications are widely used in intercontinental or intercity communications, fiber-to-the-home, and interconnections between individual computers to transmit high-bit-rate data. To address these demands, the 40–100-Gb/s Ethernet systems were standardized in 2010 [1] and the beyond 100 GbE is currently under consideration. In these systems, the optical signal sources are among the key devices. In recent high-speed modules of over 25 Gb/s, electroabsorption-modulated lasers have been typically used because they meet the requirements of speed and compactness [2]. However, direct-modulation lasers could be more attractive if they can meet the modulation-speed requirement in short-distance optical communication systems [3], [4]. In this case, the modulation speed of conventional laser diodes (LDs) is limited to approximately 40 Gb/s due to several factors, including the damping effect caused by carrier transport [5], [6]. Such damping suppresses the relaxation oscillation of LDs, thus limiting the modulation speed. To overcome this modulation limit, several types of lasers have been proposed, such as the optical injection locking techniques [7], [8] and laser with a tunnel injection structure [9]. A transistor laser (TL) is another type of directly modulated and multifunctional light sources that could meet the demands of high-speed operation above 40 Gb/s. The TL consists of a heterojunction bipolar transistor (HBT) with an active region inside the base. In the TL, the carriers are pulled from the emitter to the collector, and carrier flow passing the active region always exists. With this pulling effect, shorter carrier recovery times can be achieved, and, as a result, modulation bandwidth higher than that of conventional LDs can be expected [10]–[12]. Note that this concept was explored in 1985 using a GaInAsP/InP bulk active region [13], [14]; however, at that time, transistor operation was not achieved. Since then, the first room-temperature continuous-wave (RT-CW) transistor operation of a 0.98-μm TL has been demonstrated, and some characterizations of this transistor have been made, including transistor operations [15], [16]. At longer wavelengths, wafer design [14] and CW operation at -185 °C have been reported for a 1.5-μm-range TL, with a threshold base current of 10 mA and a current gain of 0.14 under lasing operation [17]. Our group is currently focusing on realizing 1.3-μm TLs using AlGaInAs quantum wells (QWs) with buried hetero (BH) structure, as shown in Fig. 1. In the previous reports, we successfully achieved the first RT-CW operation of a p-n-p [18] and an n-p-n TL emitting at 1.3-μm wavelength using an AlGaInAs/InP material system [19]. In this paper, details of the device structure and the fabrication processes are disclosed, and a comparison of its characteristics with those of other wafer structures is discussed. In Sections II and III, the device structure and the

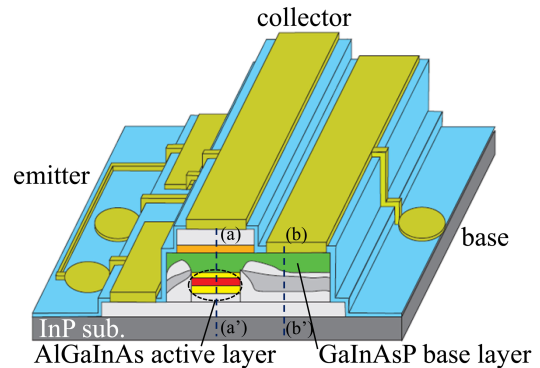

Fig. 1. Structure of an AlGaInAs/InP TL. The two dashed lines: (a)–(a′) and (b)–(b′) indicate the position of the layer structures shown in Tables I and II.

Manuscript received November 15, 2012; revised February 20, 2013; accepted February 25, 2013. Date of publication March 7, 2013; date of current version May 13, 2013. This work was supported in part by the Japan Society for the Promotion of Science under KAKENHI Grants 21226010, 22360138, 23760305, and 24246061.

N. Sato, M. Shirao, T. Sato, M. Yukinari, and N. Nishiyama are with the Department of Electrical and Electronic Engineering, Tokyo Institute of Technology, Tokyo 152-8550, Japan (e-mail: sato.n.ad@m.titech.ac.jp; shirao.m.aa@m.titech.ac.jp; sato.t.af@m.titech.ac.jp; yukinari.m.aa@m.titech.ac.jp; n-nishi@pe.titech.ac.jp).

T. Amemiya and S. Arai are with the Quantum Nanoelectronics Research Center, Tokyo Institute of Technology, Tokyo 152-8550, Japan (e-mail: amemiya.t.ab@m.titech.ac.jp; arai@pe.titech.ac.jp).

Color versions of one or more of the figures in this paper are available online at http://ieeexplore.ieee.org.

Digital Object Identifier 10.1109/JSTQE.2013.2250490

1077-260X/$31.00 © 2013 IEEE

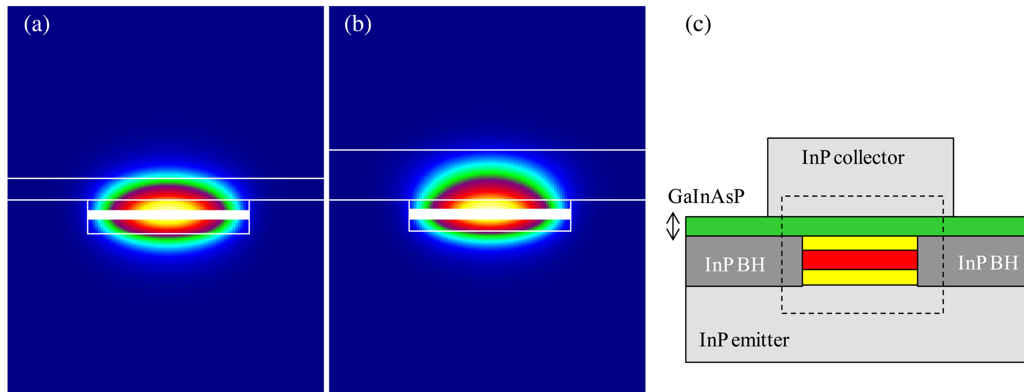

Fig. 2. Optical field of the TLs with varying base thickness (a) 200-nm-thick base. (b) 500-nm-thick base. (c) Cross-sectional drawing of the TL.

fabrication processes are explained, respectively. In Sections IV and V, the lasing and electric characteristics of p-n-p and n-p-n TLs are discussed, including the base width and thickness dependence. Finally, the discussion is concluded in Section VI.

II. Wafer Design of the TL

In previously reported short-wavelength TLs [15], [16], the waveguide structure was based on a ridge or a gain-guided waveguide structure. In these devices, CW operation was achieved with high medium gain by GaAs-based materials. Compared with such devices, the long-wavelength active materials based on InP have lower medium-gain properties and higher loss due to the Auger recombination. In addition, the optical absorption [20] of a highly doped p-type base layer was expected. Thus, realizing CW operation for long wavelength in the previous reports by other groups was difficult. To solve this problem, a BH structure was introduced in our TLs, as shown in Fig. 1. The n-p-n-p-InP current-blocking layers were regrown at both sides of the active layer. With this structure, the carrier recombination position and optical field intensity were matched, resulting in improved lasing characteristics.

Compared with conventional BH LDs [21], [22], the introduction of a base layer causes asymmetric optical mode field along the vertical direction. Therefore, calculation of the optical confinement factor of the active region was carried out. The simulated structure consisted of an InP bottom-cladding layer as emitter, five AlGaInAs QWs sandwiched by an AlGaInAs separate confinement heterostructure, a GaInAsP as the base, and an InP upper cladding as the collector. Fig. 2 shows the optical fields of the TLs with 200- and 500-nm-thick base layers. The thicker base layer pushed the optical-mode field upward (collector side), resulting in lower optical confinement in the QWs and higher optical confinement in the GaInAsP base. The optical confinement factors in the QWs with 30-, 200-, and 500-nm-thick GaInAsP bases were 5.2%, 4.9%, and 4.3%, respectively. For reference, the optical confinement of the five QWs in our conventional BH-LD was 6.2%. Thus, to realize a high-efficiency lasing operation, the GaInAsP base must be thinner.

Next, the distance between the base electrode and the active region was considered. A longer lateral current-injection distance causes higher electrical resistance; thus, the distance should be as short as possible unless the optical field overlaps

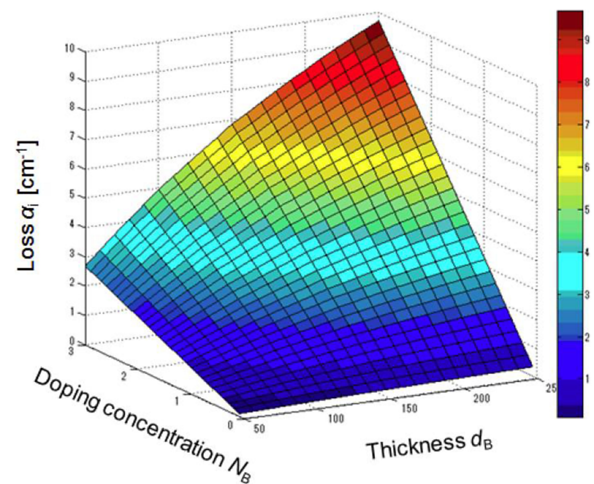

Fig. 3. Simulated additional loss by the base layers as functions of doping concentration and base thickness.

the electrode. From the numerical simulation, the lateral optical field intensity was negligible 2 μm away from the center of the active region when the width of the active region was 2 μm (1 μm each from the center). Considering fabrication tolerance, the distance was set at 4 μm in the fabrication, as will be described later.

In the final step, the doping concentration of the p-GaInAsP base N_B and the thickness of the base d_B were considered. Higher doping concentration and thicker base result in lower resistance and in higher optical absorption. Therefore, the electrical resistance and the optical absorption maintain a tradeoff relationship. Fig. 3 shows the contour plot of the additional optical internal loss that exists at the base as functions of the base doping concentration and thickness. In the calculation, the base polarity was assumed to be p-type, and the distance was 4 μm. When the base doping concentration was approximately 10^{18} cm^{-3} and the thickness was several hundred nanometers, the additional optical loss was limited in few cm^{-1} only. In addition, a thin base may result in high resistance, which degrades the lasing performance. Thus, we chose the doping concentration and thickness of 1×10^{18} cm^{-3} and $<$200 nm, respectively, in the actual device fabrication.

TABLE I
LIST OF THE LAYERS OF THE p-n-p TL STRUCTURE [LEFT: (a)–(a′). RIGHT: (b)–(b′)]

Contents	Material	Doping [cm^{-3}]	d [μm]
Contact layer	p$^+$-$Ga_{0.47}In_{0.53}As$	1.0×10^{19}	0.05
Sub-collector	p-InP	1.0×10^{18}	2
Collector layer	p- $Ga_{0.20}In_{0.80}As_{0.43}P_{0.57}$	2.0×10^{17}	0.06
Base layer	n-$Ga_{0.20}In_{0.80}As_{0.43}P_{0.57}$	2.0×10^{18}	0.2
Upper n-SCH	n- $Al_{0.27}Ga_{0.20}In_{0.53}As$	1.0×10^{17}	0.07
Upper u-SCH	u- $Al_{0.27}Ga_{0.20}In_{0.53}As$	-	0.03
TS -0.7% barrier layer ×5	u- $Al_{0.22}Ga_{0.35}In_{0.43}As$	-	0.01
CS 1.4% well layer ×5	u- $Al_{0.17}Ga_{0.10}In_{0.73}As$	-	0.005
TS -0.7% barrier layer	u- $Al_{0.22}Ga_{0.35}In_{0.43}As$	-	0.01
Bottom u-SCH	u- $Al_{0.27}Ga_{0.20}In_{0.53}As$	-	0.03
Bottom p-SCH	p- $Al_{0.27}Ga_{0.20}In_{0.53}As$	2.0×10^{17}	0.1
Bottom cladding layer	p-InP	1.0×10^{18}	0.5
Substrate	p-InP	5.0×10^{18}	350

Contents	Material	Doping [cm^{-3}]	d [μm]
Base layer	n-$Ga_{0.20}In_{0.80}As_{0.43}P_{0.57}$	2.0×10^{18}	0.2
Current blocking layer	n-InP	1.0×10^{18}	0.4
	p-InP	1.0×10^{18}	0.3
	n-InP	1.0×10^{18}	0.2
	p-InP	1.0×10^{18}	0.1
Substrate	p-InP	5.0×10^{18}	350

TABLE II
LIST OF THE LAYERS OF THE n-p-n TL STRUCTURE [LEFT: (a)–(a′). RIGHT: (b)–(b′)]

Contents	Material	Doping [cm^{-3}]	d [μm]
Contact layer	n$^+$-$Ga_{0.47}In_{0.53}As$	1.0×10^{19}	0.05
Collector layer	n-InP	1.0×10^{18}	2
Base layer	p-$Ga_{0.20}In_{0.80}As_{0.43}P_{0.57}$	1.0×10^{18}	0.030, 0.200
Upper p-SCH	p- $Al_{0.27}Ga_{0.20}In_{0.53}As$	2.0×10^{17}	0.07
Upper u-SCH	u- $Al_{0.27}Ga_{0.20}In_{0.53}As$	-	0.03
TS -0.7% barrier layer ×5	u- $Al_{0.22}Ga_{0.35}In_{0.43}As$	-	0.01
CS 1.4% well layer ×5	u- $Al_{0.17}Ga_{0.10}In_{0.73}As$	-	0.005
TS -0.7% barrier layer	u- $Al_{0.22}Ga_{0.35}In_{0.43}As$	-	0.01
Bottom u-SCH	u- $Al_{0.27}Ga_{0.20}In_{0.53}As$	-	0.03
Bottom n-SCH	n- $Al_{0.27}Ga_{0.20}In_{0.53}As$	1.0×10^{17}	0.1
Bottom cladding layer	n-InP	1.0×10^{18}	0.5
Substrate	n-InP	5.0×10^{18}	350

Contents	Material	Doping [cm^{-3}]	d [μm]
Base contact layer	p$^+$-$Ga_{0.47}In_{0.53}As$	1.0×10^{19}	0.05
Base layer	p-$Ga_{0.20}In_{0.80}As_{0.43}P_{0.57}$ (doesn't exist with modified npn TL)	1.0×10^{18}	0.2
Current blocking layer	p-InP	1.0×10^{18}	0.4
	n-InP	1.0×10^{18}	0.3
	p-InP	1.0×10^{18}	0.2
	n-InP	1.0×10^{18}	0.1
Substrate	n-InP	5.0×10^{18}	350

III. FABRICATION PROCESS

The TL fabrication process is explained in this section. The initial wafer was grown on a (1 0 0) InP substrate by organo–metallic vapor phase epitaxy (OMVPE). It consisted of a 130-nm AlGaInAs ($E_g = 1.1$ eV), 1.4% compressively strained AlGaInAs, five QWs with -0.7% tensile-strained AlGaInAs barrier layers emitting at 1.3-μm wavelength, a 100-nm AlGaInAs, a 10-nm GaInAsP ($E_g = 1.0$ eV), and an InP cap layer. The polarities of the layers depend on either the p-n-p or n-p-n TL structure. Details of the wafer structures for the p-n-p and n-p-n TLs are shown in Tables I and II, respectively. In the tables, the layer structures across (a)–(a′) and (b)–(b′) shown in Fig. 1 are summarized. Using the AlGaInAs active layer, a wide-temperature range and a high-speed operation are expected because of the material properties such as larger conduction band offset and higher differential gain compared with the GaInAsP system.

After the initial wafer growth, an InP-BH structure was formed. Because AlGaInAs compounds are known as easily oxidized materials in atmosphere, forming high-quality BH structure using regrowth is difficult [23]. To address this problem, the cleaning process, which was proven to achieve high-quality AlGaInAs BH lasers in our previous report [18], [19], was used in our TL fabrication. The cleaning process is described as follows: Mesa stripes were formed by wet etching using a bromine–methanol solution ($Br_2/CH_3OH = 1{:}1000$) and by dry etching by reactive-ion etching (RIE) using SiO_2 masks. After the mesa formation, the two cleaning processes were performed. The first wet cleaning was performed in three steps using $Br_2{:}CH_3OH$ (1:40 000) to clean the surface, $H_2SO_4{:}H_2O_2{:}H_2O$ (1:1:40) to clean the Al-containing region, and 1% BHF to remove the oxidized layer. The device was then placed in an OMVPE reactor where the second cleaning process (thermal cleaning) was conducted. We clarify that the best condition for thermal cleaning was under PH_3 atmosphere for 45 min at

650 °C [19]. When these processes were done, the mesa stripes were buried in n(100 nm)/p(200 nm)/n(300 nm)/p(400 nm)-InP current-blocking layers to form the BH structure.

After the SiO_2 selective growth mask was removed, the rest of the layers, including the base and collector layers, were regrown. Because these sequences were slightly different for each device structure, they are separately explained in Sections IV and V. Next, the collector mesa was formed by RIE and wet etching using a 200-nm-thick SiO_2 mask. An approximately 1.5-μm-high mesa was formed by RIE, and the remaining InP collector layer was removed by wet etching using hydrochloric acid solution (HCl/CH_3COOH at ratio of 1:4). After the collector mesa was formed, which had a total height of approximately 2 μm after the dry and wet etching, the mask over the collector mesa was retained, and a 100-nm-thick SiO_2 was deposited over the entire surface. Thus, the SiO_2 thickness on the collector mesa was more than 200 nm. The SiO_2 was patterned by photolithography and RIE as mask for the 34-μm-wide base-mesa formation followed by base-mesa etching using RIE. The emitter mesas were also formed in the same manner to isolate each device. The electrodes were formed in two steps. The first step formed the stripe pattern electrodes (Ti/Au: 25/200 nm) by lift off on the collector, base, and emitter mesas. The second step formed the probe pads and connected them to the electrodes. A relatively thick (approximately 4 μm thick) resist and an oblique evaporation technique were used to evaporate the metal to the side wall of the mesas. Finally, the wafer was lapped to approximately 150 μm thick, and the facets were formed by cleavage without any coating.

IV. p-n-p TL

For the first step, a "p-n-p" TL was investigated. In a p-n-p configuration, high-speed operation is difficult because the effective mass of the modulated carriers (holes) is heavy compared with that of the electrons. However, compared with an n-p-n configuration, the fabrication process is easy because the n-base ohmic contact can be formed easily.

The fabrication process is discussed in Section III. The wafer structure is shown in Table I. In this case, a 200-nm-thick n-GaInAsP base layer, a 60-nm-thick p-GaInAsP collector layer, a p-InP sub-collector layer, and a p^+-GaInAs collector contact layer were adopted for the second regrowth. In the p-n-p TLs, the n-GaInAsP base layer functioned as a base contact layer. Thus, the doping concentration of n-GaInAsP was set to a relatively high value.

Fig. 4 shows the lasing characteristics of the p-n-p TL with a common base configuration under RT-CW condition. The cavity length L is 500 μm, and the stripe width W is 1.8 μm. The solid lines indicate the light output characteristics of the common base configuration, and the dashed line indicates the light output and the $I-V$ characteristics of the two-terminal configuration (emitter–base with floating collector). The threshold current is 17 mA (threshold current density is 1.9 kA/cm^2), the external differential quantum efficiency is 47%, and the differential resistance is 6.3 Ω under the two-terminal configuration. The lasing wavelength is 1365.86 nm at $V_{\rm CB} = 1$ V. By applying the collector–base voltage $V_{\rm CB}$, the output power decreases. This phenomenon is attributed to the increase in the optical loss because of the change in the effective bandgap of GaInAsP by the collector bias (Franz–Keldysh effect) [24]. Considering that the output power of this device can be controlled by applying the collector voltage, we can expect that this device can control the gating functions by varying the collector voltage. The lasing spectrum also changes with high $V_{\rm CB}$. An approximately 2-nm sudden red shift was observed at $V_{\rm CB} = 7$ V because of the band-bending effect [18].

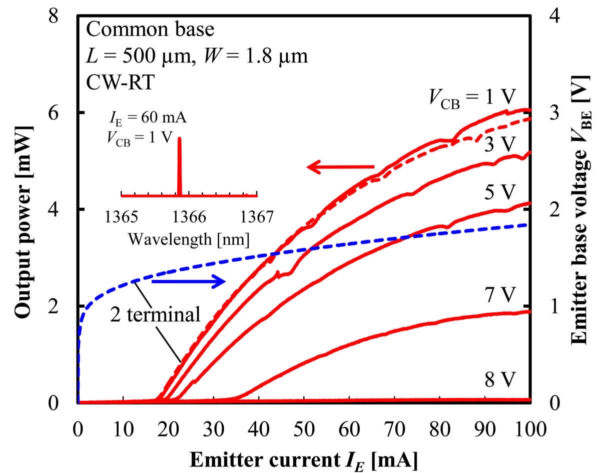

Fig. 4. Lasing characteristics and $I-V$ characteristics of a p-n-p TL under common base configuration. The inset shows the spectrum under a two-terminal configuration.

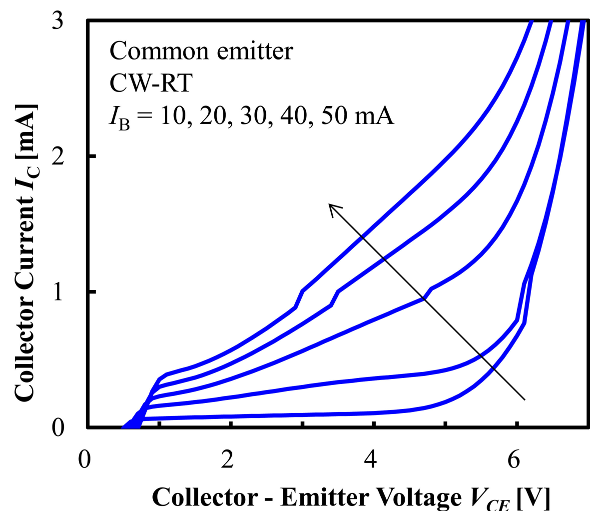

Fig. 5. $I_C-V_{\rm CE}$ characteristics of a p-n-p TL under common emitter configuration.

Fig. 5 shows the $I_C-V_{\rm CE}$ characteristics under the common emitter configuration. From the figure, the current gain, defined as I_C/I_B, is approximately 0.01 at $V_{\rm CE} = 1$ V. Despite being a very low value due to the heavy effective mass of the holes, transistor operation was achieved. At high $V_{\rm CE}$, the collector current rapidly increased because of the band bending of the base, typically observed in III–V HBTs.

Fig. 6 shows the near-field pattern below the threshold current of the p-n-p TL. A long tail emission is observed. This result indicates that the carriers that passed through the QWs recombined at the GaInAsP base. This leakage should be reduced by optimizing the structure, e.g., by reducing the base width, as described in the next section.

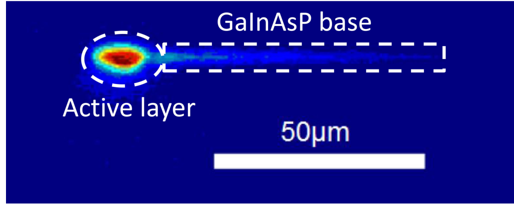

Fig. 6. Near-field pattern of the TL below the threshold current.

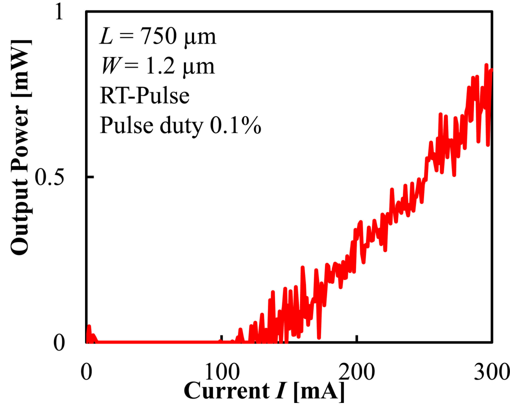

Fig. 7. Lasing characteristics of the n-p-n TL under the two-terminal configuration.

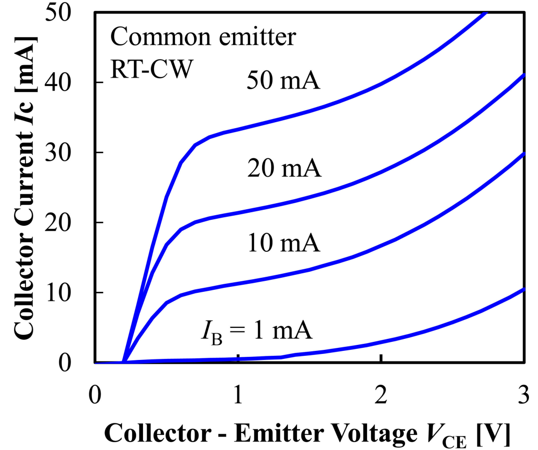

Fig. 8. $V_{\rm CE}-I_C$ characteristics of the n-p-n TL under common emitter configuration.

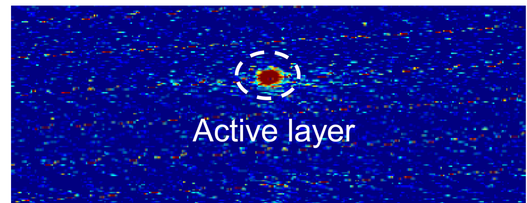

Fig. 9. Near-field pattern of the modified structure.

V. N-P-N TL

A. Original Structure

The n-p-n TL was studied. The n-p-n TL has similar structure with the p-n-p TL and the polarity of the layers is opposite (summarized in Table II). Although the QW layers were not doped in the crystal growth sequence, the QWs were actually p-doped (mid. of 10^{17} cm^{-3}) using diffusion effect of the Zn dopant, which were intentionally controlled by us to achieve n-p-n structure. The fabrication process of the n-p-n TL is more complicated than that of the p-n-p TL due to the base contact layer. In the n-p-n TL, a p$^+$-base contact layer is needed to form the ohmic contact (for the p-n-p TL, the n-GaInAsP base layer also acts as a contact layer). Up to the BH regrowth, the process is done in the same manner as that of the p-n-p TL. Thereafter, the 200-nm-thick p-GaInAsP base layer and the 50-nm-thick p$^+$-GaInAs are regrown. To prevent optical loss, the p$^+$-GaInAs contact layer just above the active layer is removed by wet etching. Then, the n-InP collector and the n$^+$-GaInAs collector contact layers are regrown.

Fig. 7 shows the light output characteristic under the two-terminal configuration. The threshold current is 120 mA, and the external differential quantum efficiency is 1% under RT-pulsed operation. No lasing was observed under the three-terminal configuration. Fig. 8 shows the $V_{\rm CE}-I_C$ characteristics under RT-CW condition. The current gain of this device, defined as I_C/I_B, was approximately 1. Compared with the p-n-p TL mentioned in the previous section, large current gain was obtained, and this difference can be explained by the difference between the effective masses of the holes and electrons. Although lasing and transistor operations were simultaneously achieved, the lasing properties became depleted compared with those of the p-n-p TL. To clarify this phenomenon, we did several measurements, which confirmed that the device had more carrier leakage at the base than that of the p-n-p TLs shown in Fig. 7 because of the higher mobility of electrons.

B. Modified Structure With Etched Base

To improve the lasing properties, we adopted a modified structure, which focused on the base region width. The modified structure had a narrow (6-μm-wide p-GaInAsP) base layer compared with the original structure mentioned previously, which had a wide base layer in the entire mesa. As shown in Fig. 6, there was a problem of the recombination at the side of the base GaInAsP layer. Thus, with the narrow base structure, the recombination at the base was expected to be suppressed; as a consequence, higher efficiency should be realized. The fabrication process was different from that of the original structure. After the regrowth of the BH structure, p-GaInAsP was regrown over the entire surface. Then, using SiO_2 mask, the p-GaInAsP base was patterned and etched off by RIE, except for the 6 μm width above the active region. The p-InP subbase layer and the p$^+$-GaInAs base contact layer were selectively regrown at both sides of the p-GaInAsP base. After the SiO_2 mask was removed, the n-InP collector and the n$^+$-GaInAs collector contact layer were regrown. The rest of the process was the same as the previous one. Fig. 9 shows the near-field pattern of the modified structure. With this structure, a better shape of the near-field pattern was confirmed with less emission from the side, in contrast to that shown in Fig. 6. This result indicates that the leakage current was reduced by the heterostructure with p-GaInAsP and p-InP.

From this modified structure, we examined two types of devices with p-GaInAsP base thicknesses of 30 and 200 nm. First, the results of the 30-nm-thick base TL are discussed. Fig. 10

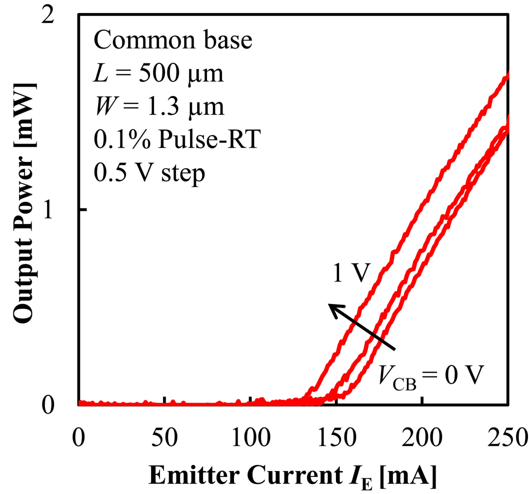

Fig. 10. Lasing characteristics of the modified n-p-n TL (30-nm base) under common base configuration.

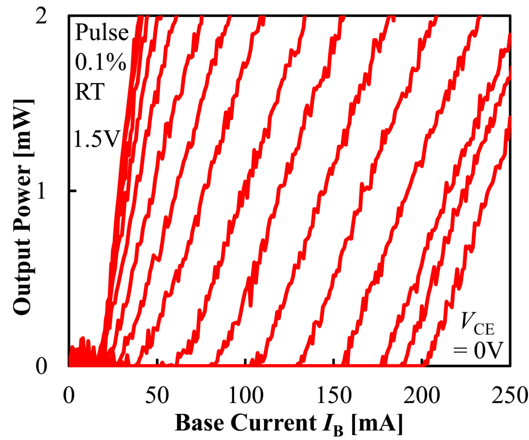

Fig. 11. Lasing characteristics of the modified n-p-n TL (30-nm base) under common emitter configuration.

shows the lasing characteristics under the common base configuration. The cavity length L is 500 μm, and the stripe width W is 1.3 μm. A threshold current of 150 mA and an external differential quantum efficiency of 3.4% with a collector–base voltage $V_{\mathrm{CB}} = 0$ V were achieved under RT-pulsed condition. Under the two-terminal configuration, the differential resistance was 16 Ω, higher than that of the p-n-p TL due to the higher resistance caused by lateral current injection in the p-type base layers. By applying the collector–base voltage V_{CB}, a little improvement in the threshold current was observed. The trend was opposite in Fig. 4. This was because of the charge of the carrier flows to the collector as applying V_{CB}. With low V_{CB}, the flow of electrons was disrupted at the base and recombined with the holes at the base, which cased insufficient holes in the QWs. With high V_{CB}, electrons were efficiently pulled out to the correct and enough holes were recombined in the QWs. Fig. 11 shows the lasing characteristics under the common emitter configuration. This measurement was also under pulsed condition, and the step of the collector–emitter voltage V_{CE} was 0.1 V. The threshold base current reached as high as 200 mA at $V_{\mathrm{CE}} = 0$ V because the recombination of electrons and holes outside the active region in the base occurred before the holes reached the

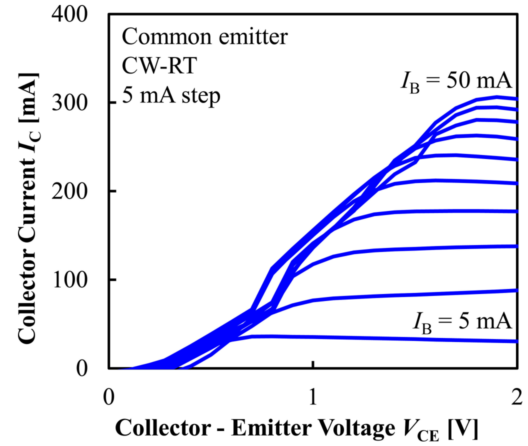

Fig. 12. $V_{\mathrm{CE}} - I_C$ characteristics of n-p-n TL (30-nm base).

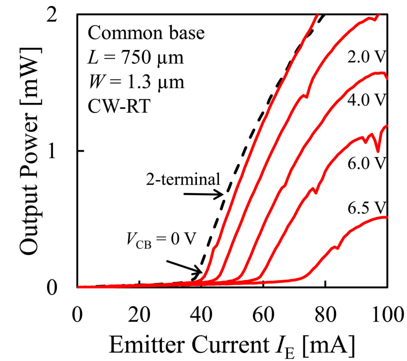

Fig. 13. Lasing characteristics of the modified n-p-n TL (200-nm base) under common base configuration.

active region owing to smaller collector current. However, the lasing properties were dramatically improved with the increase in V_{CE}, and an almost constant value under a threshold base current of 18 mA was observed above $V_{\mathrm{CE}} = 1$ V. With high V_{CE}, more electrons diffused into the collector layer, and less recombination occurred at the base. In this case, most of the injected holes from the base contributed to the lasing in the QWs. Thus, the lasing operation was controlled by the base current. Fig. 12 shows the $V_{\mathrm{CE}} - I_C$ characteristics under the common emitter configuration under RT-CW condition. The current gain, defined as I_C/I_B, was approximately 6. Using the thin base layer (30 nm thick), we successfully raised the current gain. However, a too large current gain produced extra heat; thus, no CW operation was achieved.

Fig. 13 shows the lasing characteristics of the n-p-n TL with a p-GaInAsP base thickness of 200 nm. The TL had a cavity length of 750 μm and a stripe width of 1.3 μm, and it operated under a common base configuration under RT-CW conditions. The threshold emitter current was 39 mA, whereas the external differential quantum efficiency from both facets was 13%; the calculated threshold current density was 3.5 kA/cm^2. The differential resistance was 6.7 Ω, smaller than that of the TL with a 30-nm-thick base due to the thicker base. By applying the collector–base voltage V_{CB}, both an increase in the threshold current and a decrease in the output power were observed. This phenomenon was also observed in the p-n-p TL mentioned in the previous section.

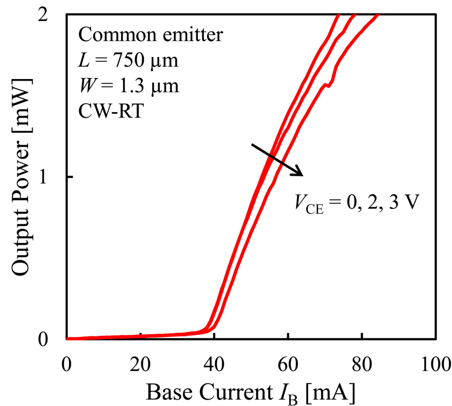

Fig. 14. Lasing characteristics of the new n-p-n TL (200-nm base) under common emitter configuration.

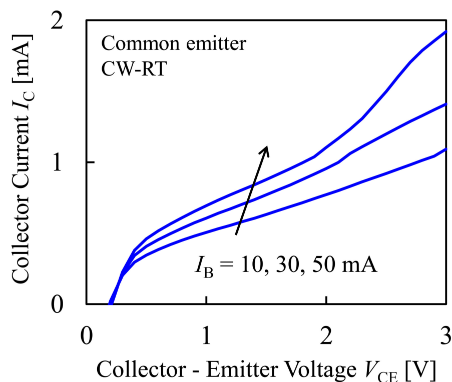

Fig. 15. $V_{CE} - I_C$ characteristics of n-p-n TL (200-nm base).

Fig. 14 shows the lasing characteristics of the device using a common emitter configuration under RT-CW condition. Almost the same threshold current (39 mA) and external differential quantum efficiency (11%) were obtained at a V_{CE} of 0 V. In contrast to the characteristics of that with the 30-nm-thick base shown in Fig. 11, minimal collector–emitter voltage dependence was observed here.

Fig. 15 shows the dependence of the collector current I_C on the collector–emitter voltage V_{CE} under the common emitter configuration. Under CW operation, the base current increased from 10 to 30 mA and then to 50 mA. Although typical transistor behavior was observed, the obtained current gain ($\beta \approx 0.02$) was much smaller than that observed in the previous results. The minimal collector–emitter voltage dependence can be explained by this small current gain.

As previously mentioned, the RT-CW operation of an n-p-n TL was achieved by suppressing the current gain. To realize high-speed operation, RT-CW operation and moderate current gain must be simultaneously achieved [25]. To enhance the TL properties, it is necessary to improve the lasing properties while maintaining the current gain. This can be realized with introduction of large bandgap and thin base layer to strengthen the carrier confinement to the QWs as well as to suppress the recombination at the base.

VI. Conclusion

In this paper, the device design and fabrication process of p-n-p and n-p-n-AlGaInAs/InP TLs emitting in the 1.3-μm wavelength region have been described, and the structural dependence of the lasing characteristics has been discussed. Controls of the lasing characteristics by the three-terminal voltage adjustment were demonstrated. Interesting characteristics were revealed, and we believe that the device performance can be made better by further investigation of the device structures toward high-speed laser operation.

Acknowledgment

The authors would like to thank Prof. M. Asada, F. Koyama, T. Mizumoto, Y. Miyamoto, and M. Watanabe of the Tokyo Institute of Technology for the fruitful discussions and support.

References

[1] IEEE 802.3b Standard [Online]. Available: http://www.ieee802.org/3/ba/

[2] T. Fujisawa, S. Kanazawa, L. Takahata, W. Kobayashi, and T. Tadokoro, “Ultra-high-speed electroabsorption modulator integrated lasers for 100 GbE and beyond,” in *Proc. 17th Opto-Electron. Commun. Conf.*, 2012, pp. 75–76.

[3] M. Matsuda, T. Simoyama, A. Uetake, S. Okumura, M. Ekawa, and T. Yamamoto, “Uncooled, low-driving-current 25.8 Gbit/s direct modulation using 1.3 μm AlGaInAs MQW distributed-reflector lasers,” *Electron. Lett.*, vol. 48, no. 8, pp. 450–452, Apr. 2012.

[4] W. Kobayashi, T. Tadokoro, T. Ito, T. Fujisawa, T. Yamanaka, Y. Shibata, and M. Kohtoku, “High-speed operation at 50 Gb/s and 60-km SMF transmission with 1.3-μm InGaAsAs-based DML,” in *Proc. IEEE Int. Semicond. Laser Conf.*, 2012, pp. 50–51, Paper TuB1.

[5] R. Nagarajan, M. Ishikawa, T. Fukushima, R. S. Geels, and J. E. Bowers, “High speed quantum-well lasers and carrier transport effects,” *IEEE J. Quantum Electron.*, vol. 28, no. 10, pp. 1990–2008, Oct. 1992.

[6] S. C. Kan, D. Vassilovski, T. C. Wu, and K. Y. Lau, “Quantum capture limited modulation bandwidth of quantum well, wire, and dot lasers,” *Appl. Phys. Lett.*, vol. 62, no. 19, pp. 2307–2309, May 1993.

[7] X. Zhang, A. Gutierrez-Aitken, D. Klotzkin, P. Bhattacharya, C. Caneau, and R. Bhat, “0.98-μm multiple-quantum-well tunneling injection laser with 98-GHz intrinsic modulation bandwidth,” *IEEE J. Sel. Topics Quantum Electron.* vol. 3, no. 2, pp. 309–314, Apr. 1997.

[8] Y. Higa, T. Miyamoto, H. Nakajima, K. Fujimoto, and F. Koyama, “Theoretical design of carrier injection rate and recombination rate in tunnel injection quantum-well lasers,” *Physica Status Solidi(c)*, vol. 5, no. 9, pp. 2838–2840, 2008.

[9] Z. Lingxiao and J. P. Leburton, “Modeling of the transient characteristics of heterojunction bipolar transistor lasers,” *IEEE J. Quantum Electron.*, vol. 45, no. 4, pp. 359–366, Apr. 2009.

[10] J. Shibata, Y. Mori, Y. Sasai, N. Hase, H. Serizawa, and T. Kajiwara, “Fundamental characteristics of an InGaAsP/InP laser transistor,” *Electron. Lett.*, vol. 21, no. 3, pp. 98–100, Jan. 1985.

[11] B. Faraji, S. Wei, D. L. Pulfrey, and L. Chrostowski, “Analytical modeling of the transistor laser,” *IEEE J. Sel. Topics Quantum Electron.*, vol. 15, no. 3, pp. 594–603, May/Jun. 2009.

[12] M. Shirao, S. Lee, N. Nishiyama, and S. Arai, “Large-signal analysis of a transistor laser,” *IEEE J. Quantum Electron.*, vol. 47, no. 3, pp. 359–367, Mar. 2011.

[13] Y. Mori, J. Shibata, Y. Sasai, H. Serizawa, and T. Kajiwara, “Operation principle of the InGaAsP/InP laser transistor,” *Appl. Phys. Lett.*, vol. 47, no. 7, pp. 649–651, Oct. 1985.

[14] M. Feng, N. Holonyak, A. James, K. Cimino, G. Walter, and R. Chan, “Carrier lifetime and modulation bandwidth of a quantum well AlGaAs/InGap/GaAs/InGaAs transistor laser,” *Appl. Phys. Lett.*, vol. 89, no. 11, pp. 113504-1–113504-3, Sep. 2006.

[15] M. Feng, N. Holonyak, H. W. Then, and G. Walter, “Charge control analysis of transistor laser operation,” *Appl. Phys. Lett.*, vol. 91, no. 5, pp. 053501-1–053501-3, Jul. 2007.

[16] Z. Duan, W. Shi, L. Chrostowski, X. Huang, N. Zhou, and G. Chai, “Design and epitaxy of 1.5-μm InGaAsP-InP MQW material for a transistor laser,” *Opt. Exp.*, vol. 18, no. 2, pp. 1501–1509, Jan. 2010.

[17] F. Dixon, M. Feng, N. Holonyak, Jr., Y. Huang, X. B. Zhang, J. H. Ryou, and R. D. Dupuis, “Transistor laser with emission wavelength at 1544 nm,” *Appl. Phys. Lett.*, vol. 93, no. 15, pp. 021111-1–021111-3, Jul. 2008.

[18] M. Shirao, T. Sato, Y. Takino, N. Sato, N. Nishiyama, and S. Arai, “Lasing operation of long-wavelength transistor laser using AlGaInAs/InP

quantum well active region," in *Proc. 23rd Int Conf. Indium Phosphide Related Mater.*, May 2011, pp. 1–4.
[19] N. Sato, M. Shirao, T. Sato, M. Yukinari, N. Nishiyama, T. Amemiya, and S. Arai, "Room-temperature continuous wave operation of a 1.3-μm npn-AlGaInAs/InP transistor laser," in *Proc. 23rd IEEE Int. Semicond. Laser Conf.*, Oct. 2012, pp. 18–19.
[20] B. Jensen, "Quantum theory of free carrier absorption in polar semiconductors," *Ann. Phys.*, vol. 80, no. 2, pp. 284–360, 1973.
[21] Y. Takino, M. Shirao, T. Sato, N. Nishiyama, T. Amemiya, and S. Arai, "Regrowth interface quality dependence on thermal cleaning of AlGaInAs/InP buried-heterostructure lasers," *Jpn. J. Appl. Phys.*, vol. 50, no. 7, pp. 070203-1–070203-3, Jul. 2011.
[22] Y. Takino, M. Shirao, N. Sato, T. Sato, T. Amemiya, N. Nishiyama, and S. Arai, "Improved regrowth interface of AlGaInAs/InP-buried-heterostructure lasers by in-situ thermal cleaning," *IEEE J. Quantum Electron.*, vol. 48, no. 8, pp. 971–979, Aug. 2012.
[23] K. Takemasa, M. Kubota, and H. Wada, "1.3-μm AlGaInAs buried-heterostructure lasers," *IEEE Photon. Tech. Lett.*, vol. 11, no. 8, pp. 941–951, Aug. 1999.
[24] D. A. B. Miller, D. S. Chemla, and S. Schmitt-Rink, "Relation between electroabsorption in bulk semiconductors and in quantum wells: The quantum-confined Franz–Keldysh effect," *Phys. Rev. B*, vol. 33, no. 10, pp. 6976–6982, 1986.
[25] M. Shirao, N. Nishiyama, N. Sato, and S. Arai, "Theoretical analysis of the damping effect on transistor lasers," *IEICE Electron. Exp.*, vol. 9, no. 23, pp. 1792–1798, 2012.

Noriaki Sato was born in Shizuoka Prefecture, Japan, in 1988. He received the B.E. degree from the Tokyo Institute of Technology, Tokyo, Japan, in 2011, where he is currently working toward the Master's degree.

His research interest is focused on the improvement of buried heterolaser characteristics in the AlGaInAs material system.

Mr. Sato is a member of the Japan Society of Applied Physics.

Mizuki Shirao (S'08–M'12) received the B.E., M.E., and Ph.D. degrees in electrical and electronic engineering from the Tokyo Institute of Technology, Tokyo, Japan, in 2007, 2009, and 2011, respectively.

He joined Mitsubishi Electric Co., Ltd., Tokyo, in 2011. His research interests include long-wavelength transistor lasers and terahertz modulation by optical signals.

Dr. Shirao is a member of the Japan Society of Applied Physics.

Takashi Sato was born in Ibaraki Prefecture, Japan, in 1987. He received the B.E. and M.E. degrees from the Tokyo Institute of Technology, Tokyo, Japan, in 2010 and 2012, respectively.

His research interest is focused on the fabrication processes of long-wavelength transistor lasers. He has been with the Nippon Telegraph and Telephone East Corporation, Tokyo, since 2012.

Mr. Sato is a member of the Japan Society of Applied Physics.

Masashi Yukinari was born in Kanagawa Prefecture, Japan, in 1989. He received the B.E. degree from the Tokyo Institute of Technology, Tokyo, Japan, in 2012, where he is currently working toward the Master's degree.

His research interest is focused on the improvement of transistor laser characteristics.

Nobuhiko Nishiyama (M'01–SM'07) was born in Yamaguchi Prefecture, Japan, in 1974. He received the B.E., M.E., and Ph.D. degrees from the Tokyo Institute of Technology, Tokyo, Japan, in 1997, 1999, and 2001, respectively. During his Ph.D. work, he demonstrated the single-mode 0.98 and 1.1-μm vertical-cavity surface-emitting laser (VCSEL) arrays with stable polarization using misoriented substrates for high-speed optical networks, as well as metal–organic chemical vapor deposition-grown GaInNAs VCSELs.

He joined Corning, Inc., NY, USA, in 2001, where he was with the Semiconductor Technology Research Group. At Corning, Inc., he was involved in several subjects, including short-wavelength lasers, 1060-nm DFB/DBR lasers, and long-wavelength InP-based VCSELs. Since 2006, he has been an Associate Professor at the Tokyo Institute of Technology. His current interests are focused on transistor lasers, silicon photonics, III–V silicon hybrid optical devices, and terahertz-optical signal conversions involving optics–electronics–radio integration circuits.

Dr. Nishiyama is a member of the Japan Society of Applied Physics, Institute of Electronics, Information and Communication Engineers (IEICE), and IEEE Photonics Society. He is the Chair of the technical group of silicon photonics in IEICE. He received the Excellent Paper Award from IEICE of Japan in 2001 and the Young Scientists Prize in the Commendation for Science and Technology from the Ministry of Education, Culture, Sports, Science and Technology in 2009.

Tomohiro Amemiya (S'06–M'09) received the B.S., M.S., and Ph.D. degrees in electronic engineering from the University of Tokyo, Tokyo, Japan, in 2004, 2006, and 2009, respectively.

In 2009, he moved to the Quantum Electronics Research Center, Tokyo Institute of Technology, where he is currently an Assistant Professor. His research interests include the physics of semiconductor light-controlling devices, metamaterials for optical frequency, magnetooptical devices, and in the processing technologies for fabricate these devices.

Dr. Amemiya is a member of the Optical Society of America, the American Physical Society, and the Japan Society of Applied Physics. He received the 2007 IEEE Photonics Society Annual Student Paper Award and the 2008 IEEE Photonics Society Graduate Student Fellowships.

Shigehisa Arai (M'83–SM'06–F'10) was born in Kanagawa Prefecture, Japan, in 1953. He received the B.E., M.E., and D.E. degrees in electronics from the Tokyo Institute of Technology, Tokyo, Japan, in 1977, 1979, and 1982, respectively. During his Ph.D. work, he demonstrated room-temperature continuous-wave operations of 1.11–1.67-μm long-wavelength lasers fabricated by liquid-phase epitaxy, as well as their single-mode operation under rapid direct modulation.

He joined the Department of Physical Electronics, Tokyo Institute of Technology as a Research Associate in 1982 and joined AT&T Bell Laboratories, Holmdel, NJ, USA, as a Visiting Researcher from 1983 to 1984, on leave from the Tokyo Institute of Technology. He became a Lecturer in 1984, an Associate Professor in 1987, and a Professor with the Research Center for Quantum Effect Electronics and the Department of Electrical and Electronic Engineering in 1994. Since 2004, he has been a Professor with the Quantum Nanoelectronics Research Center, Tokyo Institute of Technology. His research interests include photonic integrated devices such as dynamic-single-mode and wavelength-tunable semiconductor lasers, semiconductor optical amplifiers, and optical switches/modulators. His current research interests include studies on low-damage and cost-effective processing technologies of ultrafine structures for high-performance lasers and photonic integrated circuits on silicon platforms.

Dr. Arai is a member of the Optical Society of America, the Institute of Electronics, Information and Communication Engineers (IEICE), and the Japan Society of Applied Physics (JSAP). He received an Excellent Paper Award from the IEICE of Japan in 1988, the Michael Lunn Memorial Award from the Indium Phosphide and Related Materials Conference in 2000, Prizes for Science and Technology including a Commendation for Science and Technology from the Minister of Education, Culture, Sports, Science and Technology in 2008, an Electronics Society Award and the Achievement Award from IEICE in 2008 and 2011, respectively, and a JSAP Fellowship in 2008.